Supporting Information

Bifunctional Non-precious Metal Electrocatalysts of Porous WO_2 Hexahedral Networks for Full Water Splitting

Chang Shu,[a] Shuai Kang,[a] Yanshuo Jin,[a] Xin Yue[a] and Pei Kang Shen*[ab]

[a] State Key Laboratory of Optoelectronic Materials and Technologies, School of Materials Science and Engineering, Sun Yat-sen University, Guangzhou 510275, P. R. China

[b] Collaborative Innovation Center of Renewable Energy Materials, Guangxi Key Laboratory of Electrochemical Energy Materials, State Key Laboratory of Processing for Non-ferrous Metal and Featured Materials, Guangxi University, Nanning 530004, P. R. China.

*E-mail: pkshen@gxu.edu.cn

Additional experimental data

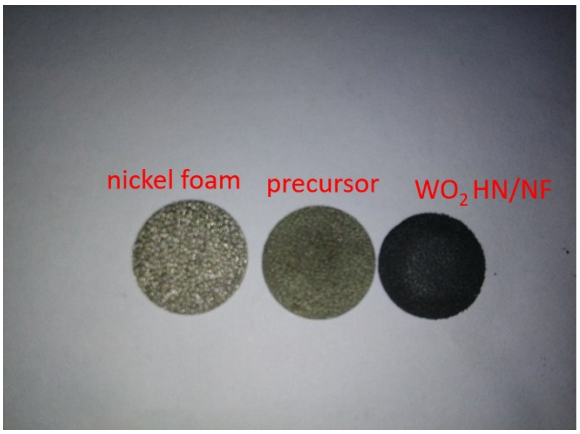

Figure S1. Photographs of the nickel foam (left), the precursor (middle) and WO_2 HN/NF (right).

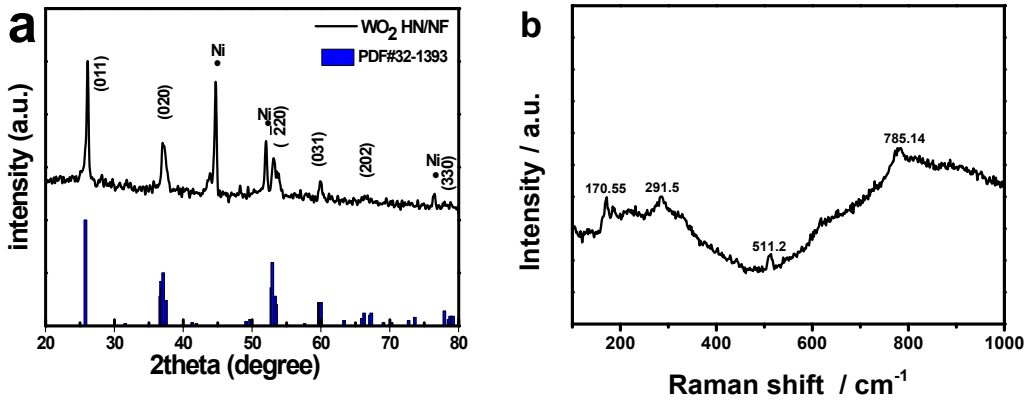

Figure S2. (a) XRD pattern of WO_2 HN/NF (black dot indicates nickel element). (b) Raman spectrum of WO_2 HN/NF.

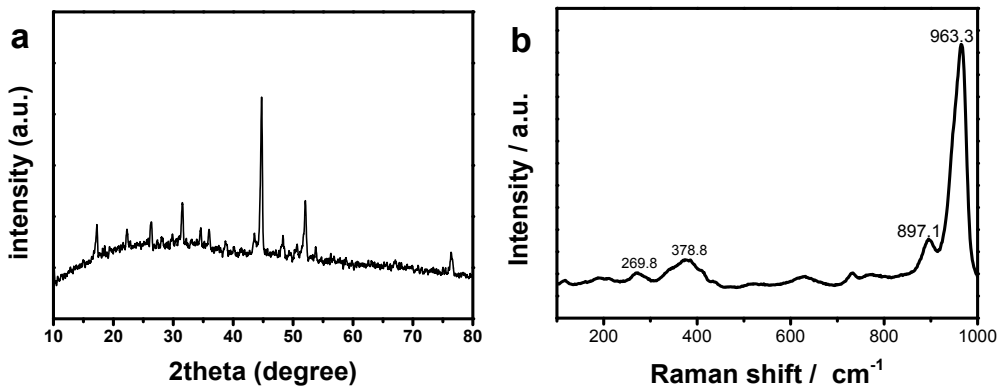

Figure S3. (a)The XRD pattern of the precursor. (b) Raman spectra of the precursor.

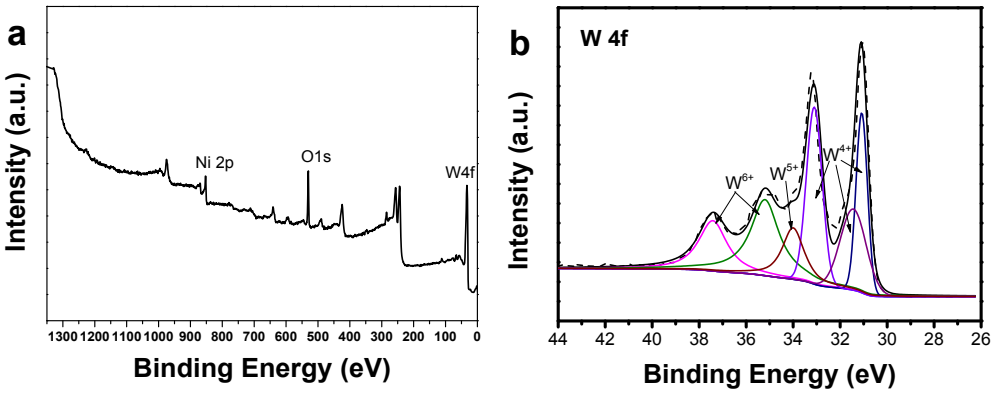

Figure S4. XPS spectra of WO_2 HN/NF. (a) Survey scan curves. (b) W 4f peaks.

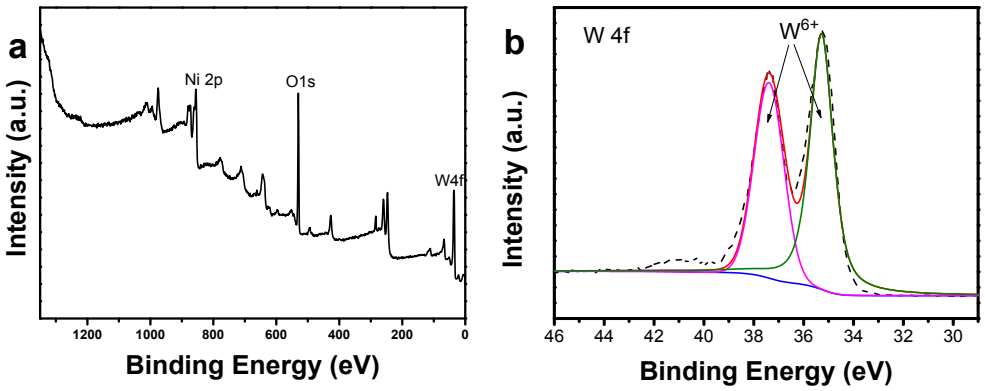

Figure S5. XPS spectra of WO_3/NF. (a) Survey scan curves. (b) W 4f peaks.

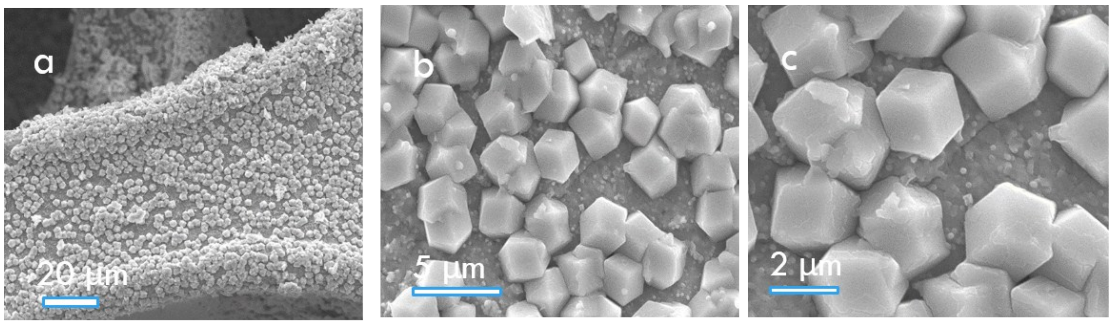

Figure S6. The SEM of the precursor.

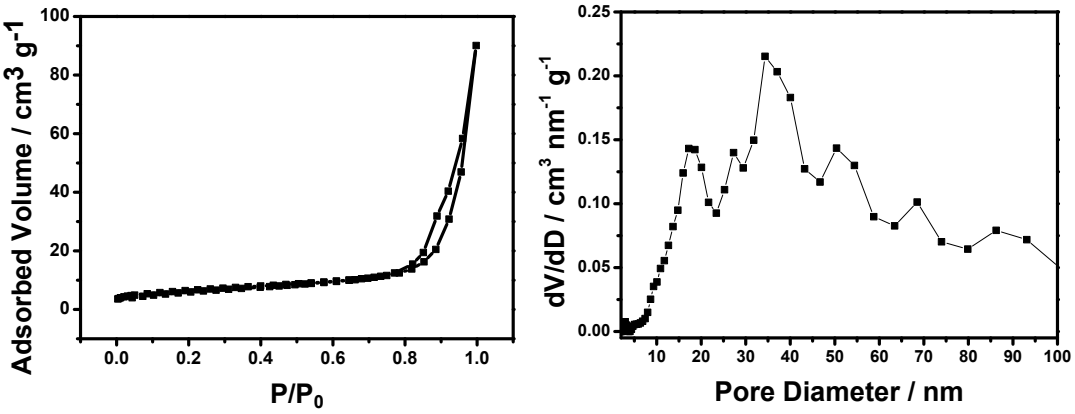

Figure S7. N_2 adsorption-desorption isotherms of porous WO_2 HN/NF (left) and the corresponding pore size distribution of porous WO_2 HN/NF (right).

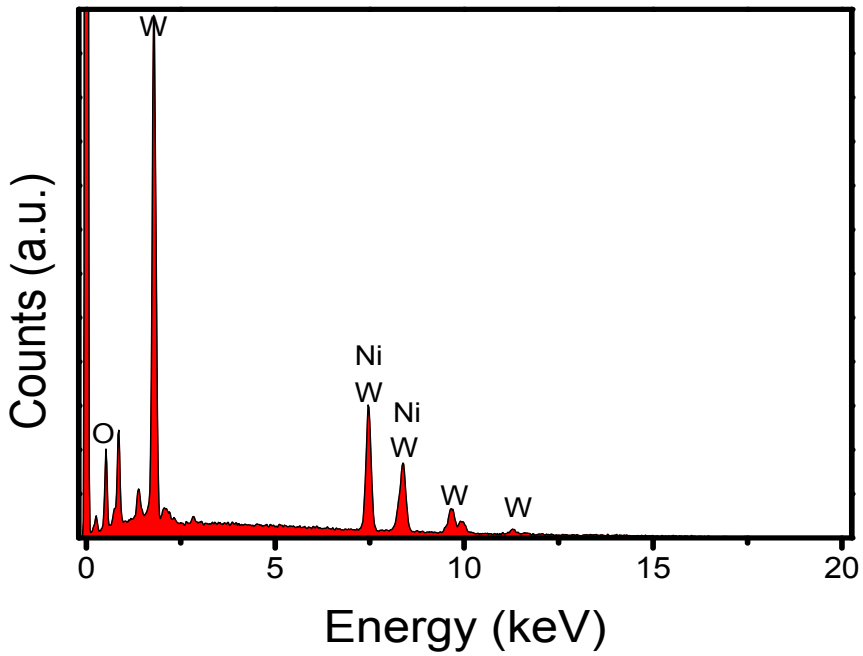

Figure S8. EDX spectrum of porous WO_2 hexahedral networks supported on nickel foam.

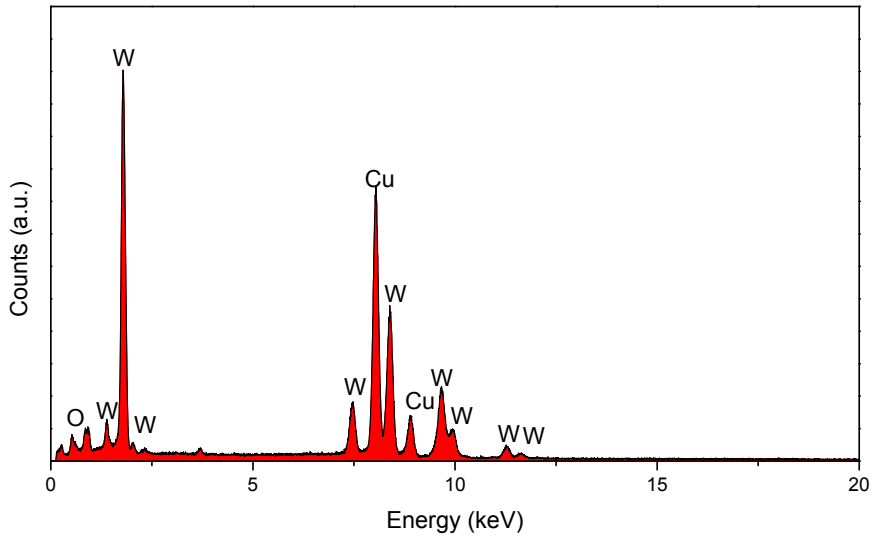

Figure S9. EDX spectrum of WO_2 hexahedral networks supported on nickel foam.

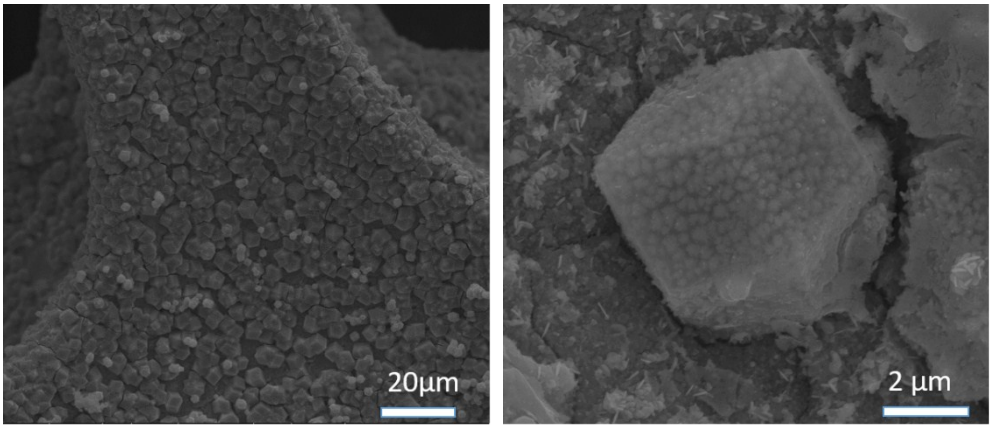

Figure S10. The morphology image of porous WO_2 HN/NF after HER.

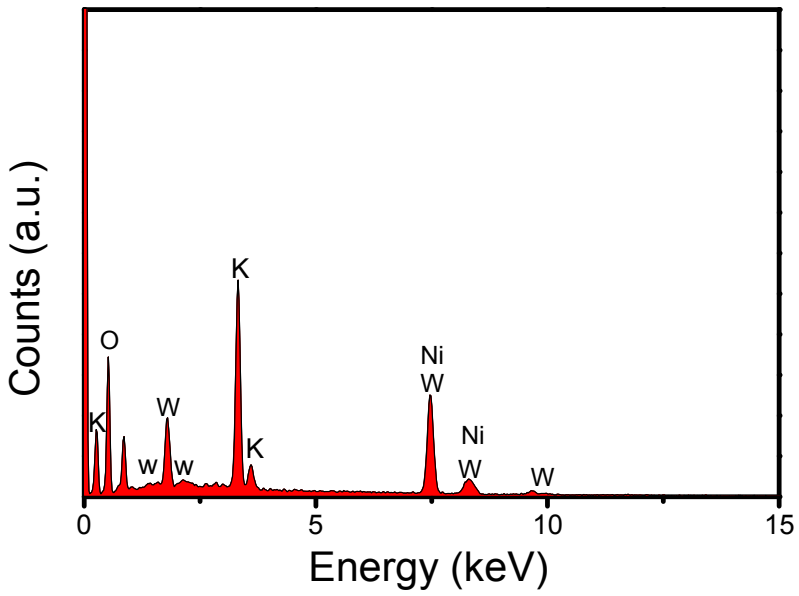

Figure S11. EDX spectrum of porous WO_2 HN/NF after electrochemical test.

Molecular models and band structures of WO_2

The model of WO_2 was established by deleting one of the tungsten atoms, as shown in Figure S12. The dimension of such a unit cell is 7.14 Å × 7.14 Å × 20 Å with sufficient vacuum space in Z direction to separate the interaction between periodic images. A Gamma centred 10×10×1 *K*-point mesh was used to sample the Brillouin zone for geometry optimization, and 40 *K*-points along each high-symmetry line in the Brillouin zone were used to obtain band structure. The cut-off energies for plane waves were chosen to be 500 eV, and the convergence tolerance of force on each atom during structure relaxation was set to be 0.001 eV/Å. Polarization effect was considered in all cases.

Active sites and adsorption properties

The free energy of the adsorbed state is calculated as

$\Delta G_{H^*} = \Delta E_{H^*} + \Delta E_{ZPE} - T\Delta S$

where ΔE_{H^*} is the hydrogen chemisorption energy (either integral or differential), and ΔE_{ZPE} is the difference corresponding to the zero point energy between the adsorbed state and the gas phase. As the vibrational entropy of H* in the adsorbed state is small, the entropy of adsorption of ½ H_2 is $\Delta S_H \approx -\frac{1}{2}S^0_{H2}$, where S^0_{H2} is the entropy of H_2 in the gas phase at the standard conditions. Therefore the overall corrections are taken as in

$\Delta G_{H^*} = \Delta E_{H^*} + 0.24\ eV$

The exploration of HER active sites was conducted by placing a hydrogen atom above each W atom of the WO_2 as shown in Figure S13;

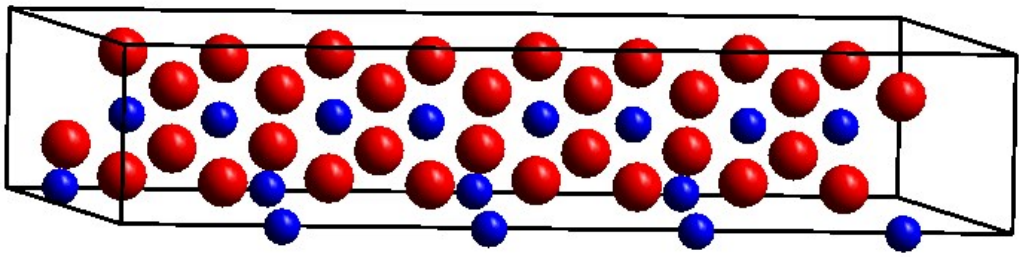

Figure S12. The model is a 1×1×4 cell along the [011] direction. Blue balls represent tungsten atoms and red balls represent O atoms.

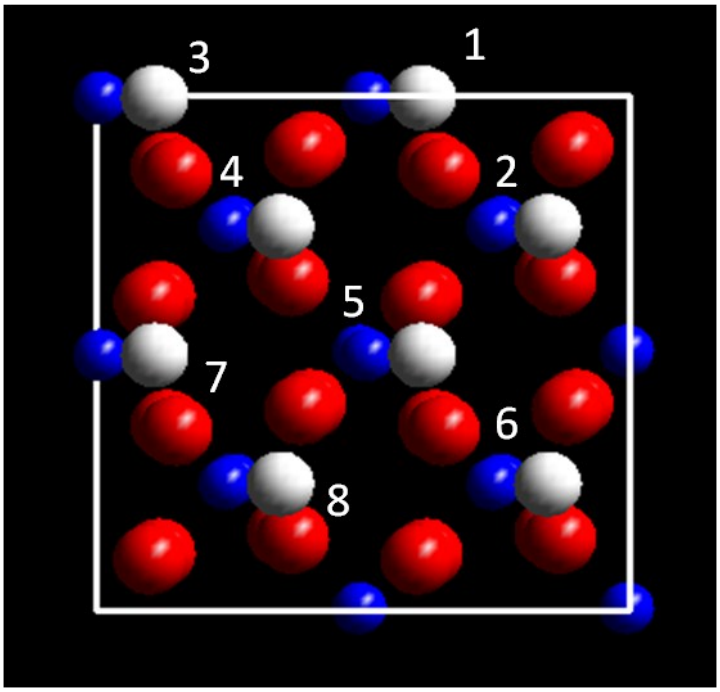

Figure S13. We put H atoms at the top of W atoms. White balls represent H atoms. There are 8 sites. We have calculated several combinations.

According to the formula: $\Delta E_{H^*} = E_{tot} - E_{cat} - E_H$[1], we have come to this conclusion. The results comparing current catalysts are shown in the following figure.

Table S1 Hydrogen Adsorption Energy (ΔE_{H^*}) on Different Electrocatalysts for HER

	ΔE_{H^*} (eV)	ΔG_{H^*} (eV)	Ref.
Pt	-0.33	-0.09	2
Ir	-0.21	0.03	2
Mo	-0.61	-0.37	2
W	-0.67	-0.43	2
MoS_2	-0.16	0.08	1
WO_2	-0.32	-0.08	This work

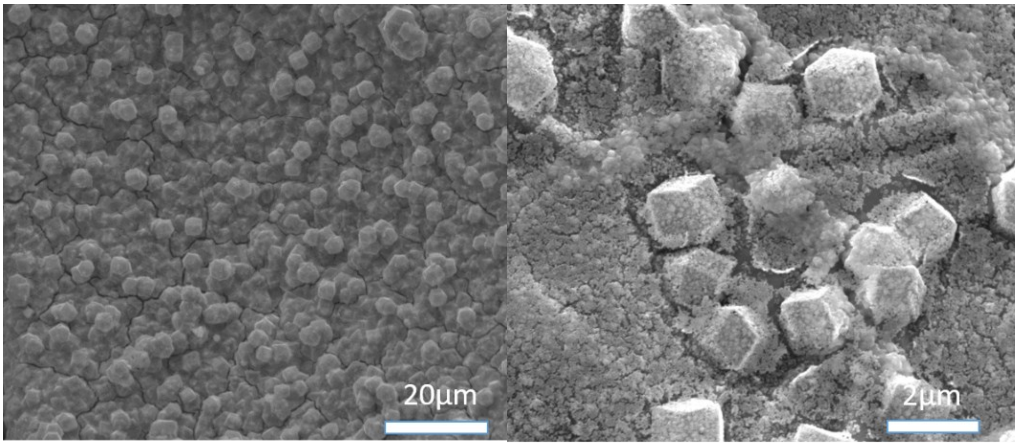

Figure S14. The morphology image of porous WO_2 HN/NF after OER.

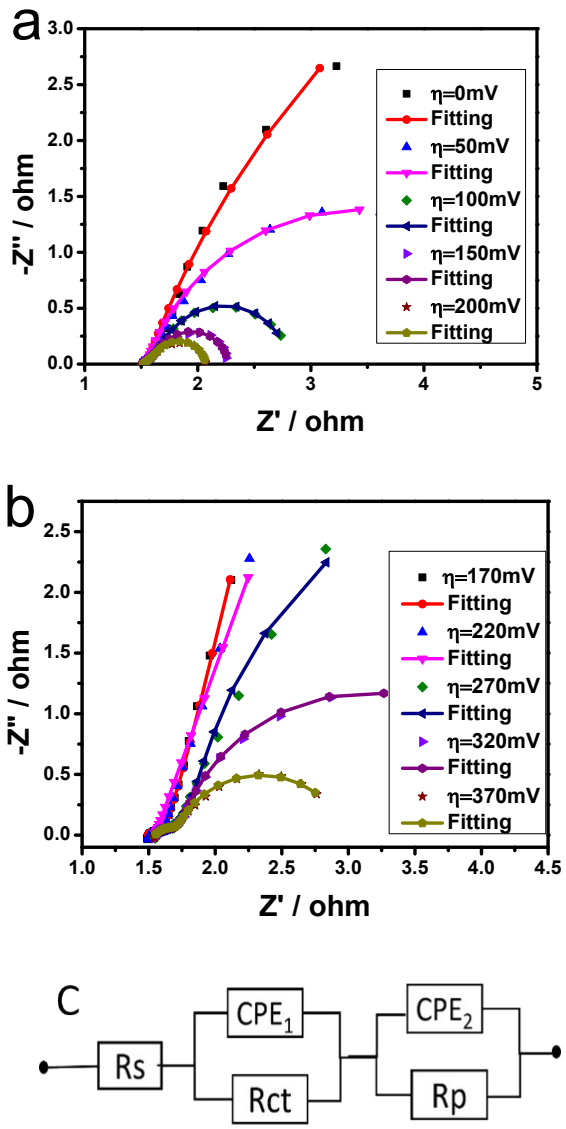

Figure S15. (a) The Nyquist plots of porous WO_2 HN/NF for HER at η=0, 50, 100, 150 and 200 mV (b) The Nyquist plots of porous WO_2 HN/NF for OER at η=170, 220, 270, 320 and 370 mV (c) The electrical equivalent circuit is used to model the system of the catalysts

Synthesis of Control group /Ni: This is a control experiment, and we put Ni foam with pretreatment in 30 mL distilled water. Then they are transferred to a 50 mL Teflon lined stainless steel reaction vessel. The other conditions not change. Finally, the samples are annealed 1 h at 600 °C in H_2.

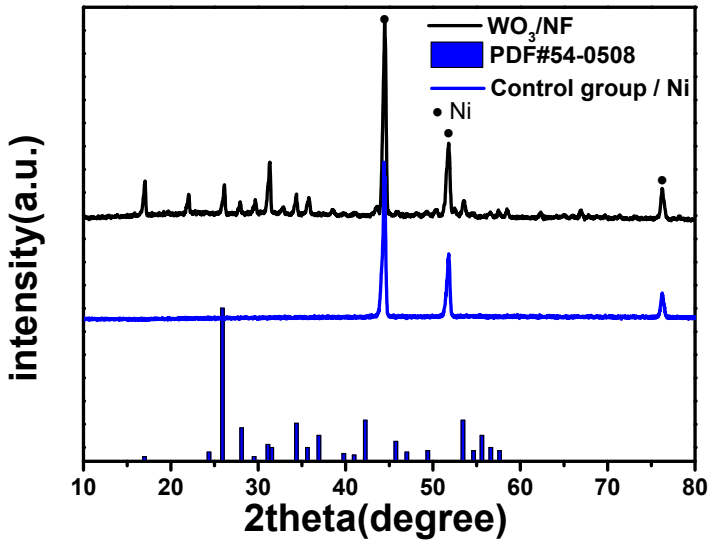

Figure S16. The XRD pattern of WO_3/NF.

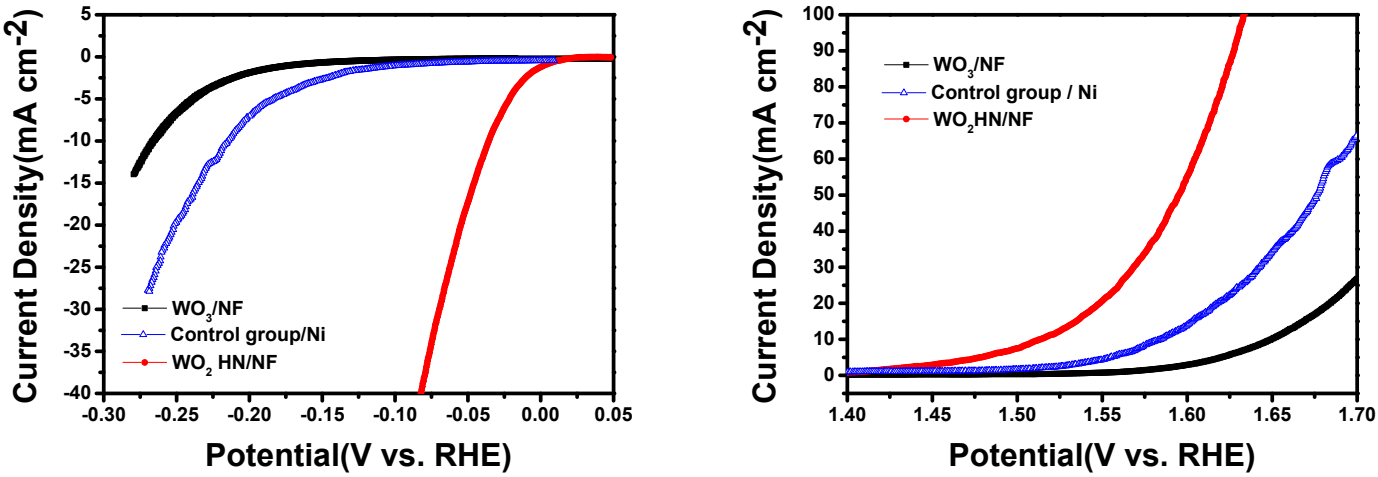

Figure S17. Polarization curves of WO_3/NF, and WO_2 HN/NF for HER (left) and OER (right) in 1 M KOH.

The precursor shows the current density of -10 mA cm^{-2} at an overpotential of 286 mV for HER and 10 mA cm^{-2} at an overpotential of 380 mV for OER in alkaline electrolyte

(1.0 M KOH). In contrast, porous WO_2 HN/NF has more excellent electrochemical performance than precursor.

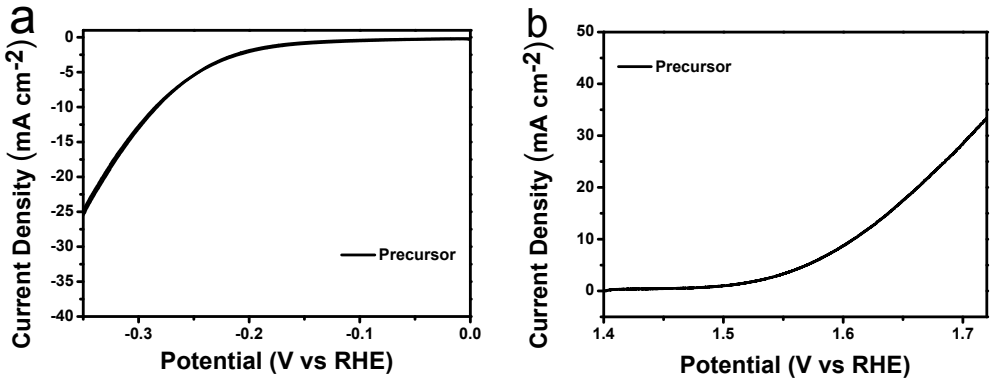

Figure S18. Polarization curves of precursor for HER (left) and OER (right) in 1 M KOH.

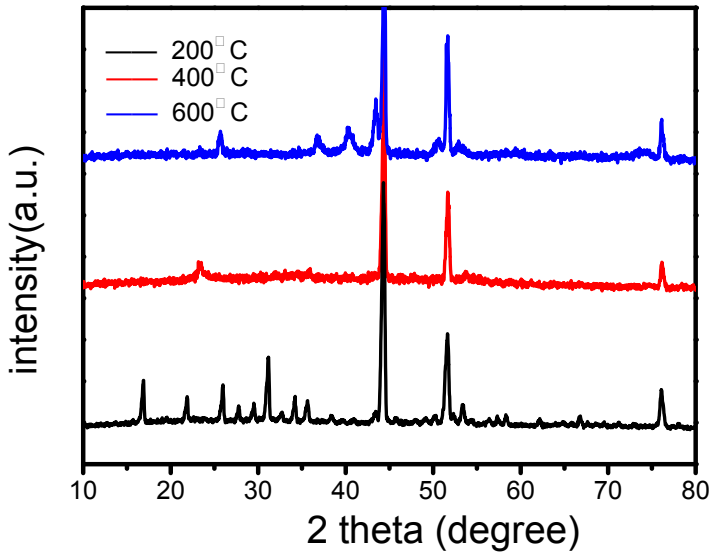

Figure S19. XRD patterns of the precursor at different temperatures in H_2 atmosphere.

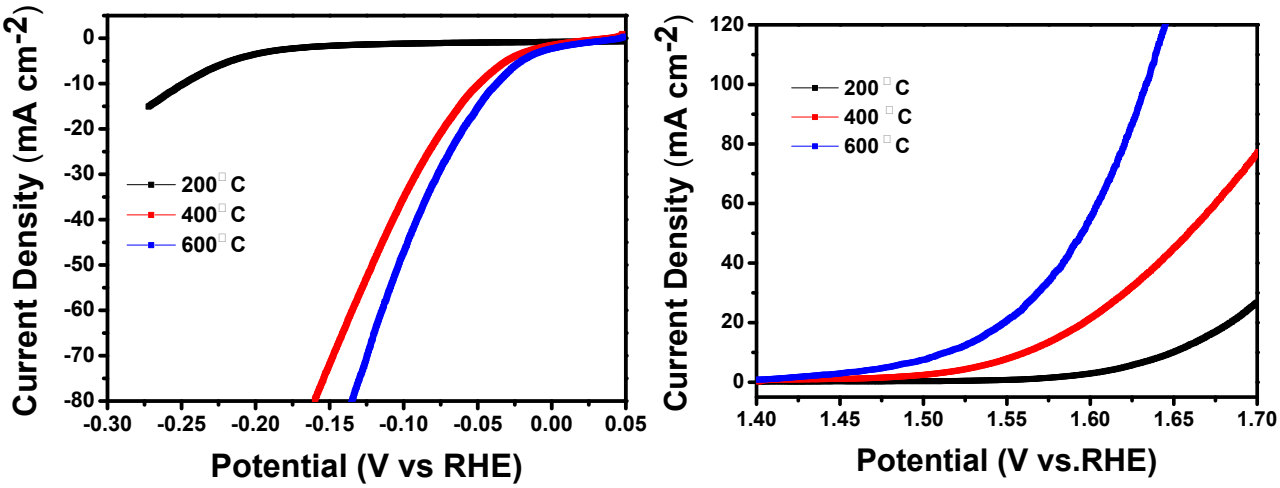

Figure S20. Polarization curves of samples at different temperatures (200 °C, 400 °C, 600 °C) for HER (left) and OER (right) in 1 M KOH.

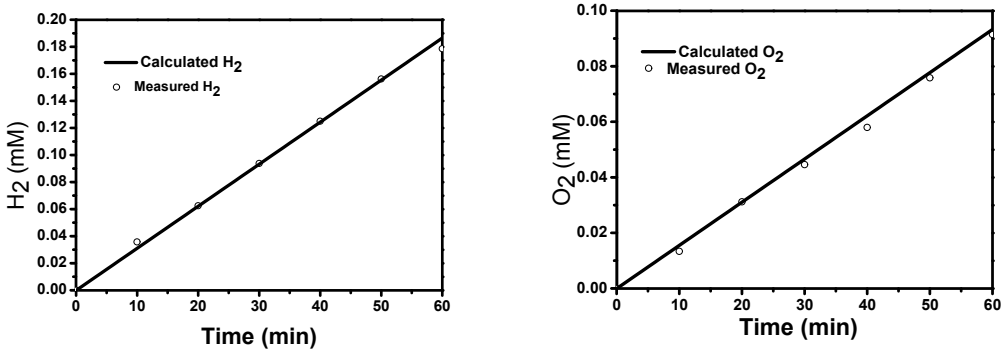

Figure S21. The amount of H_2 / O_2 theoretically calculated and experimentally measured versus time for both HER and OER of porous WO_2 HN/NF. The current density is 10 mA cm^{-2} for 1 hours.

Table S2. HER, OER and full water splitting activities of the porous WO_2 HN/NF, and reported catalysts.

Catalyst	Electrolyte	HER Potential vs. RHE (V) @ 10 mA cm^{-2}	OER Potential vs. RHE (V) @ 10 mA cm^{-2}	Full Water Splitting Potential (V) @ 10 mA cm^{-2}	Reference
Ni_2P/Ni/NF	1.0 M KOH	-0.098	1.43	1.49	3
Ni_5P_4 Films/Ni foil	1.0 M KOH	-0.15	1.56	Below 1.7	4
Ni_3S_2/NF	1.0 M KOH	-0.223	1.49	~1.76(@ ~13 mA cm^{-2})	5
$Fe_{10}Co_{40}Ni_{40}P$/NF	1.0 M KOH	-0.068	1.48	1.57	6
NiSe /Ni foam	1.0 M KOH	-0.096	1.5 (@ ~20 mA cm^{-2})	1.63	7
Compact MoO_2/NF	1.0 M KOH	-0.124	1.59	1.73	8
MWCMNs[a]	0.5 M H_2SO_4	-0.056			1
d-WSe_2/CFM[b]	0.5 M H_2SO_4	-0.228			9
G-WS_2/Ti plate[c]	0.5 M H_2SO_4	-0.306			10
Porous WO_2 HN/NF	1.0 M KOH	-0.048	1.5	1.59	This work

a: Metallic WO_2−Carbon Mesoporous Nanowires

b: 3D dendritic WSe_2 on conductive carbon nanofiber mats

c: graphene film-confined WS_2 nanoparticles

1. R. Wu, J. F. Zhang, Y. M. Shi, D. Liu and B. Zhang, *Journal of the American Chemical Society*, 2015, **137**, 6983-6986.
2. J. K. Nørskov, T. Bligaard, A. Logadottir, J. R. Kitchin, J. G. Chen, S. Pandelov and U. Stimming, *Journal of The Electrochemical Society*, 2005, **152**, J23.
3. B. You, N. Jiang, M. L. Sheng, M. W. Bhushan and Y. J. Sun, *ACS Catal.*, 2016, **6**, 714-721.
4. M. Ledendecker, S. K. Calderon, C. Papp, H. P. Steinruck, M. Antonietti and M. Shalom, *Angew. Chem. Int. Ed.*, 2015, **54**, 12361-12365.
5. L.L. Feng, G. Yu, Y. Wu, G.-D. Li, H. Li, Y. Sun, T. Asefa, W. Chen and X. Zou, *J. Am. Chem. Soc.*, 2015, **137**, 14023-14026.
6. Z. Zhang, J. Hao, W. Yang and J. Tang, *RSC Adv.*, 2016, **6**, 9647-9655.
7. C. Tang, N. Y. Cheng, Z. H. Pu, W. Xing and X. P. Sun, *Angew. Chem. Int. Ed.*, 2015, **54**, 9351-9355.
8. Y. S. Jin, H. T. Wang, J. J. Li, X. Yue, Y. J. Han, P. K. Shen and Y. Cui, *Adv. Mater.*, 2016, **28**, 3785-3790.
9. M. L. Zou, J. F. Zhang, H. Zhu, M. L. Du, Q. F. Wang, M. Zhang and X. W. Zhang, *J. Mater. Chem. A*, 2015, **3**, 12149-12153.
10. Z. H. Pu, Q. Liu, A. M. Asiri, A. Y. Obaid and X. P. Sun, *Electrochim. Acta*, 2014, **134**, 8-12.